Analysis of Pseudo-Turbulence Flow Induced by Bubble Periodic Formation in Non-Newtonian Fluids

Fan, Wenyuan*[+]; Yin, Xiao Hong

School of Chemistry and Chemical Engineering, Tianjin University of Technology, No391 Binshui West Road, Xiqing District, Tianjin 300384, P.R. CHINA

ABSTRACT: *Laser Doppler Velocimetry (LDV) has been employed to determine pseudo-turbulence characteristics of the flow field around bubble train forming in non-Newtonian caboxymethylcellulose (CMC) aqueous solution at low gas flow rate condition. The Reynolds stress and turbulent intensity of the liquid were investigated by means of Reynolds time-averaged method. The experimental results show that axial Reynolds stress rises greatly and then fluctuates slightly with the vertical height, whereas displays symmetrical Gaussian distribution in the horizontal direction; Radial Reynolds stress changes nonobviously in the vertical direction, but increases followed by a decrease in the horizontal direction. The axial turbulent intensity begins to wave to some degree with the height for near vertical axis passing through orifice center, but maintains constant within bubble channel in the horizontal direction; Radial turbulent intensity gets down with the vertical height, compared with the opposite trend of its variation with the horizontal distance.*

KEYWORDS: *Non-Newtonian fluid; Bubble train; Laser Doppler velocimetry; Pseudo-turbulence.*

INTRODUCTION

Gas-liquid two-phase bubbly flows in non-Newtonian fluids have been widely encountered in many industrial applications, such as chemical, biochemical, environmental, petrochemical processes [1]. In very common gas-liquid contactors which usually employ bubbly flow, such as bubbles column and bioreactor [2, 3], bubble formation is frequently carried out (e.g., hydrogenation, desulfurization, Fischer-Tropsch synthesis, etc.). This dispersion process will not only create significant characteristics of a bubble, such as a bubble shape, size, velocity, and track but also cause marked changes in the flow fields around bubbles in non-Newtonian fluids, which consequently lead to a distinct impact on the mass and heat transfer between gas-liquid phases. On the other hand, the critical Reynolds number beyond which bubbles change their behavior is far lower than the well-known value under the bubble formation and its initial rising stages [4]. However, the local turbulence induced by bubble chain forming in fluid, so-called pseudo-turbulence [5], can enhance phase interaction and influence the trajectories of bubbles, so as to improve greatly the mass and heat transfer rate between two-phase within the contactors. Therefore, an adequate understanding of pseudo-turbulence flow induced by bubble formation as well as rising in non-Newtonian fluid is essential for proper design and optimization of gas-liquid contactors under industrial condition.

* *To whom correspondence should be addressed.*
+ *E-mail: wyfan@tjut.edu.cn*
1021-9986/2018/5/167-175 *9/$/5.09*

A large number of studies have been reported on a topic related to bubble formation through a single orifice or a single nozzle., but most of them have focused on Newtonian fluids [6] and only a few have considered non-Newtonian fluids. For example, several researchers have investigated bubble characteristics (e.g., size, shape, frequency) [7-9] during its formation process, the corresponding influences (e.g., fluids properties, physical geometry, operating conditions) [10-12] on them, and various prediction models for bubble size or shape [13-16]. Specifically, by introducing the state equation of ideal, *Martín et al.* [17,18] has satisfactorily predicted the bubble volume, superficial area and bubble shape using a non-spherical model in both water and CMC aqueous solution., Based on considering the effect of the ingoing gas throughout orifice, *Ma et al.* [19] has successfully developed a novel model for calculating the bubble size and. Even more, *Vélez-Cordero* and *Zenit* [20] devoted to the bubble cluster formation in shear-thinning fluids, but concerned mostly the mean rise velocity of the bubbles with respect to the velocity achieved by single bubbles or Newtonian fluids.

As it is well known, most of the above studies on bubble dynamics in non-Newtonian fluids are high associated with the flow fields around a deforming bubble. However, a few types of research concerned the relevant studies on flow fields and were frequently interested in bubble wake formed behind the leading bubble and its effect on trailing bubble, as well as its difference from that in Newtonian fluids. A negative wake in non-Newtonian fluids was firstly observed to push the liquid away from the bubble by *Hassager* [21]. Subsequently, by means of Laser Doppler Anemometry (LDA), *Bisgaard* and *Hassager* [22] concluded that a negative wake was induced by the elasticity of fluids, which usually has the opposite-direction effect to the inertial force. This peculiar feature has also been observed for spheres falling in viscoelastic liquids [23]. By using Particle Image Velocimetry (PIV), *Frank* and *Li* [24,25] found while bubbles or spheres rise in polyacrylamide (PAM) solutions, there exist three zones: a central downward flow behind the bubble (negative wake), a conical upward flow surrounding the negative wake zone, and an upward flow zone in front of the bubble. *Sousa et al.* [26] focused on the interaction between two consecutive Taylor bubbles rising in non-Newtonian solutions via sets of laser diodes/photocells and PIV, and found that for the less concentrated CMC solutions, the interaction between Taylor bubbles was similar to that found in Newtonian fluids, but for the most concentrated CMC solution, a negative wake forms behind the Taylor bubbles. *Lin* and *Lin* [27] devoted to the coalescence mechanism of in-line two-unequal bubbles rising in PAM solution using Particle Image Analyzer (PIA) and pointed out that the acceleration of the trailing bubble to the leading one should be attributed to the dragging force caused by the negative pressure and the shear-thinning effect, and also the pushing force caused by the viscoelastic effect. *Fan et al.* [28] investigated the interaction between two parallel rising bubbles by analyzing the velocity field around bubbles using PIV.

Although the previously reported literature of flow field reveals some interesting features of the phenomenon, there is still little information available on the fundamental formation process. To get detailed characteristics of the flow field around a bubble, both during initial formation and later rising process in non-Newtonian fluids is critical to understand adequately bubble formation mechanism and bubble interaction theory as well as coalescence regime. But meanwhile, owing to the merits of high resolution, noninterference, quick response, and wide range, LDV has become one of the most favored optical measurement techniques for gas-liquid two-phase flow application compared to the conventional one-point measurement tool, such as Pitot tube, hot wire anemometry, etc. The LDV system is more robust for optical disturbances even at higher mixture velocities, compared with PIV system, which, however, gets invalid for the interface at higher mixture velocities due to large reflections created by interfacial waves and droplets [29]. In this work, the pseudo-turbulence flow features of a periodic bubble generation and rise in shear-thinning CMC aqueous solution will be investigated by analysis the mean velocity, Reynolds stress and turbulent intensity in both radial direction and axial direction using LDV, respectively.

EXPERIMENTAL SECTION

Experimental setup

The experimental set-up consists of a single bubble generation system and a LDA measurement system, as shown in Fig. 1. In the bubble generation system, a square

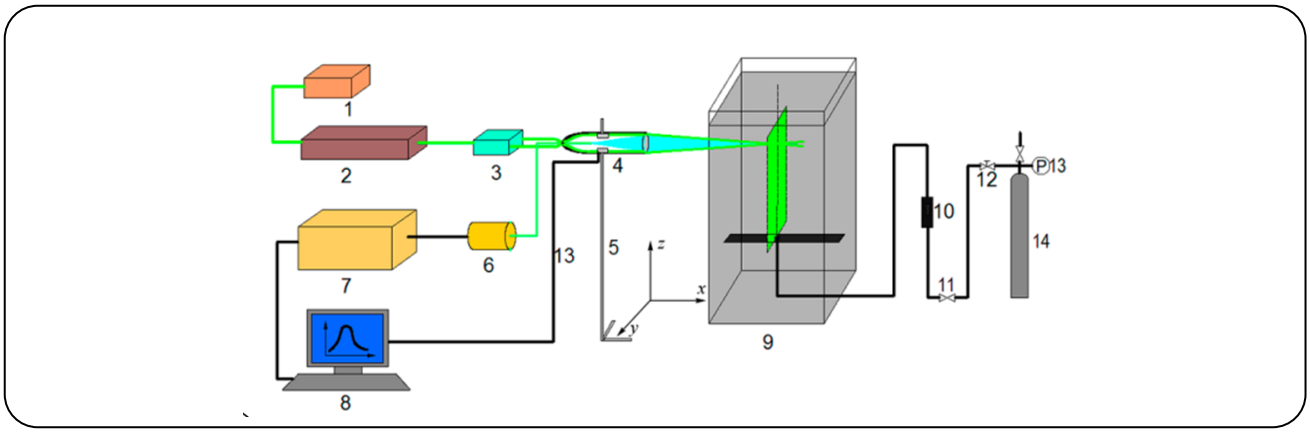

Fig. 1: Schematic representation of the experimental setup. 1: cooling system; 2: laser; 3: Bragg cell; 4: transmitting and receiving optics; 5: 3D coordinate frame; 6: photo multiplier; 7: BSA signal processor; 8: computer; 9: PMMA square tank; 10: rotameter; 11: valve; 12: pressure maintaining valve; 13: manometer; 14: nitrogen cylinder.

PMMA tank with inner dimension 15×15×50cm, which was considered to be large enough and allow neglecting the effect of the wall on the shape and size of bubbles, was used basically. A PMMA plate (15×5 cm cross-section and 1 cm thick) with a polished orifice (inner diameter 1 mm) at its center was built inside the tank 10 cm above the bottom for generating bubbles. A stainless steel tube with an inner diameter 2 mm was employed to connect the nitrogen cylinder, the rotamete, and the orifice. Taking into account the pressure range inside the bubble, nitrogen pressure was maintained at little more than 0.1 MPa by adjusting a regulation valve, thus gas flow rate could be displayed accurately by the calibrated rotameter. Bubbles were always generated individually by adjusting the gas flow rate properly.

In LDV measurement system (DANTEC, Fiber flow series 60X, Denmark), a 5W water-cooled argon-ion laser source, a multi-color beam separator, a fiber optic probe with a focal length of 310 mm, a multi-color receiver coupled with a traversing coordinate, a signal processor (Dantec 57N21), a personal computer and the Burst Spectrum Analyzer (BSA) Flow Software 2.1 for data acquisition, were used in the liquid velocity measurement. The backscatter mode in a cell-free system and a pre-shift frequency of 40 kHz were adopted respectively. The vertical component was determined with green (λ=514.5nm) beams and the horizontal component with blue (λ=488nm) beams. A reasonable amount of spherical glass particles with a mean diameter of about 10μm (ρ=1.5×103 kg/m^3) was added and distributed homogeneously in the whole solution. These seeding particles carried by the liquid reflect the laser light toward the photo-detector probe, which can convert the light into electrical signals, and therefore, the liquid velocity was obtained using a signal processor by the special software. At each measuring point, the data was usually taken for 180s.

Test section

In particular, the bubble shape takes symmetric with the axis of the vertical line passing through orifice center, and it rises up straightly without any obvious swinging under the experimental conditions. Thence, only velocities in both *y* direction and *z* direction need to be considered whereas the velocity neglected in the *x* direction. Finally, by considering the overall factors including bubble characteristics and the fluid properties, the test section was selected as a rectangular area with the following geometric parameters: width (in the *y* direction) *W*=1.6cm, height (in *z* direction) *H*=7.85cm, as illustrated in Fig. 2. Especially, to avoid the influence of refraction of PMMA cross-section with the orifice on the laser beam, the origin (*O*) of the co-ordinate system was set at the intersection point of the vertical line passing through orifice center and the horizontal line 2.0 mm above the orifice. The *x*-axis was perpendicular to the above test section, the *y*-axis was parallel to the horizontal direction, and the *z*-axis lies upright in the gas flow direction along the vertical axis passing through the orifice center. The velocity components corresponding to the {*x*, *y*, *z*} axes were denoted as {*u*, *v*, *w*}, respectively.

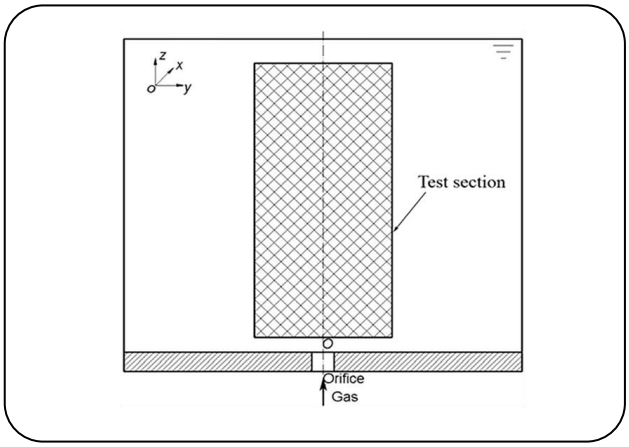

Fig. 2: Schematic diagram of the test section.

Experimental conditions

The setup described above was employed to determine the velocity fields of liquid around a growing and rising bubble in CMC aqueous solution under following conditions: orifice diameters: 2.0 mm; gas flowrate: 0.5mL/s; mass concentrations of CMC aqueous solution: 0.15%. The rheological parameters of CMC aqueous solutions were measured by Rheometer of StressTech (REOLOGICA Instruments AB, Sweden), and the results show the behavior of shear-thinning of the fluid can be described very well by Carreau model [30] under experimental shear rang($0.8\sim500s^{-1}$). Therefore, by fitting above rheological using this model, the relevant parameters were obtained as follows: zero shear viscosity (η_0): 0.0376 Pa·s, infinite shear viscosity (η_∞): 0.001 Pa·s, time constant (λ): 0.0690 s, and flow index (n): 0.808.

Calculation of Reynolds stresses and turbulent intensity

In this work, the fluid pseudo-turbulence induced by a cyclical bubble generation at a submerged orifice can be calculated from the temporal variations of instantaneous liquid velocities at a given position. Furthermore, the velocity components *w* and *v* in the axial direction (*z*-axis) and radial direction (*y*-axis) respectively are considered whereas velocity component *u* is negligible based on the aforementioned reasons (Test section). Mean velocity components are computed by the following formula.

$$\begin{cases} \bar{v} = \dfrac{1}{N}\sum_{i=1}^{N} v(i) \\ \bar{w} = \dfrac{1}{N}\sum_{i=1}^{N} w(i) \end{cases} \tag{1}$$

Where **v**(i), w(i) and $\bar{v}$, $\bar{w}$ are instantaneous velocity components and mean velocity components. The parameter *N* is the total number of coincident points at a specified measurement node.

The Reynolds stresses are given as Eq. (2).

$$\begin{cases} \overline{v'v'} = \dfrac{1}{N}\sum_{i=1}^{N}\left(v(i)-\bar{v}\right)\left(v(i)-\bar{v}\right) \\ \overline{w'w'} = \dfrac{1}{N}\sum_{i=1}^{N}\left(w(i)-\bar{w}\right)\left(w(i)-\bar{w}\right) \end{cases} \tag{2}$$

The turbulent intensities (*I*) are calculated from the root mean square of the turbulent fluctuation of the instantaneous liquid velocities.

$$\begin{cases} I_y = \dfrac{\sqrt{\overline{v'v'}}}{\bar{v}} \\ I_z = \dfrac{\sqrt{\overline{w'w'}}}{\bar{w}} \end{cases} \tag{3}$$

RESULTS AND DISCUSSION

The instantaneous velocity time series of liquids obtained from LDV, with its intense pulsation as shown in Fig. 3, are firstly calculated by Reynolds time-averaged method using MatLab software to acquire the mean velocity in the axial and radial direction in the test section. Then the axial and radial Reynolds stress distributions, as well as turbulent intensity distributions, are then discussed so as to discover the turbulent flow characteristics during the bubble formation process and ultimately improve the mass and heat transfer rate between gas-liquid.

Reynolds stress distribution

By substituting the mean velocity components into Eq. (2) and (3), the magnitudes of Reynolds stress and turbulent intensity at the measurement node can be gained respectively. Fig. 4 shows the variation curve of axial Reynolds stresses with the vertical height (a) and horizontal distance (b). As can be found that within a certain horizontal distance (e.g. *y*=0, 2mm), axial Reynolds stress increases rapidly with the vertical height and then fluctuates around a constant value. It can be inferred that throughout bubble generating and rising process, there might exist a cylindrical bubble channel, vertical to the test section and axisymmetrical with

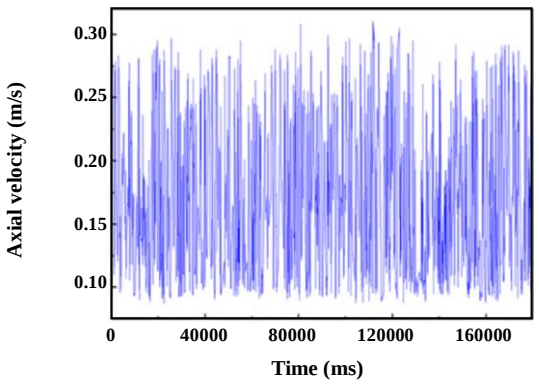

Fig. 3: Part of the instantaneous time series of axial velocity.

the central axis line passesing through orifice center since bubble in the CMC aqueous solution ascends steadily along a straight path with no swinging motions. Therefore, the above changes of axial Reynolds stress indicate that there exists the larger fluctuation in the axial component of liquid velocity within this channel, but a somewhat diminished tendency at the edge of this channel. Consequently, with the vertical height, both the growth rate and finally constant value of axial Reynolds stress deduce correspondingly. Until y=8mm, the pulse of the axial component of liquid velocity almost disappeared, resulting in zero value of in axial Reynolds stress, as shown in Fig. 4 (a). Furthermore, the variation of axial Reynolds stresses exhibits an approximate Gauss distribution with the horizontal distance, and enhances with vertical height, as shown in Fig. 4 (b). Actually, on the one hand, during the bubble formation process, the fluctuations of axial velocity caused by bubble interface disturbance always decrease with the angle between the velocity vector and the symmetrical axis, while this angle increase with the horizontal distance around the bubble surface during its growth. On the other hand, during the bubble rising process, the flow resistance of liquid decreases significantly with the horizontal distance due to the shear-thinning effect of CMC solution induced by the leading bubble, resulting in a rapid rise of liquid axial velocity as well as its pulsation there. In addition, at the larger height, it is easier to get larger axial velocity and its fluctuation which is induced by bubble acceleration after its departure from the orifice. So, Reynolds stress in axial component goes up with vertical height.

Fig. 5 presents the corresponding radial Reynolds stress varying with vertical heights and horizontal distance. It is shown that the radial Reynolds stress almost maintains the zero value in the bubble channel near the vertical symmetrical axis (e.g. y=0.0, 2.0mm), compared with the intensified pulsation of liquid near the boundary of the bubble channel (e.g. y=4.0, 6.0mm). This is because the liquid flow near the central axis, induced by bubble inertia motion, almost moves upward, leading to small radial velocity as well as slight pulsation. But near the boundary of the above channel, the turbulence of the liquid is strengthened by the high-speed shear effect of the bubble, consequently resulting in the large fluctuation in radial Reynolds stress. However, for further large distance from the symmetrical axis (e.g. y=8.0mm), the liquid pulsation gets down again owing to the decreasing bubble-induced flow, as shown in Fig. 5 (a). It is also indicated that with the horizontal distance, radial Reynolds stress grows first and then deduces, resulting in the saddle-shaped curves symmetrical along with the aforementioned symmetrical axis. Especially, except for maximum value on the boundary of the bubble channel, radial Reynolds stresses at different height become almost unchangeable.

Turbulent intensity distribution

Fig. 6 depicts that axial turbulent intensity varies with the vertical height (a) and the horizontal distance (b). It can be revealed that in the case of low height (bubble formation process, e.g. z = 0~13mm), axial turbulent intensity induced by axial disturbance manifests a certain degree of volatility with the vertical height because axial Reynolds stress begins to fluctuate upward and downwards with the height in this under-formation range. However, by contrast, in the case of high height (bubble rising process, e.g. z=18~78mm), axial Reynolds stress hardly changes with the vertical height, thus axial turbulent intensity always maintains zero with the height accordingly, as shown in in Fig.6 (a). But for low height situations, there occurs a complex fluctuation in radial turbulent intensity, while this fluctuation is gradually intensified with the horizontal distance for high situations.

In a word, turbulent intensity shows strong volatility with the increase of vertical height, but indeed, there are still some rules on its variation in the horizontal direction to follow: Axial turbulent intensity almost keeps constant within bubble channel, whereas fluctuation appears only at the boundary of the bubble channel. Besides, radial

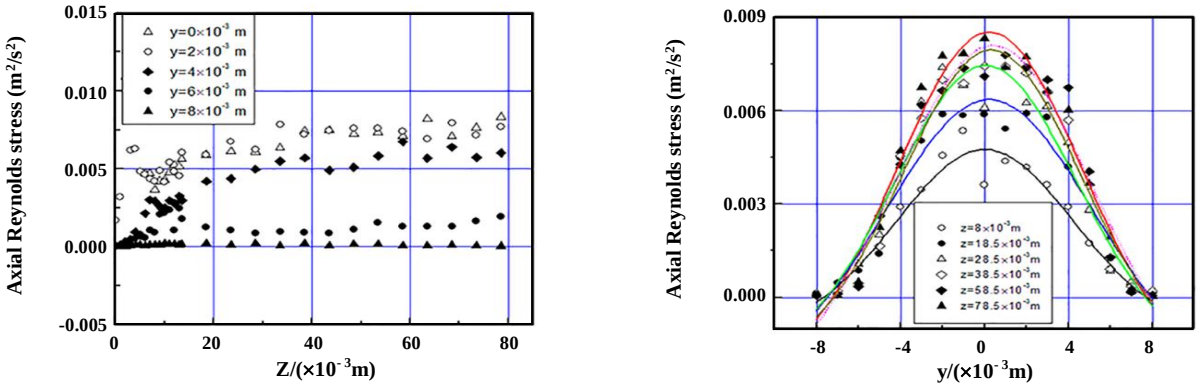

Fig. 4: Axial Reynolds stress varies with heights (a) and horizontal positions (b).

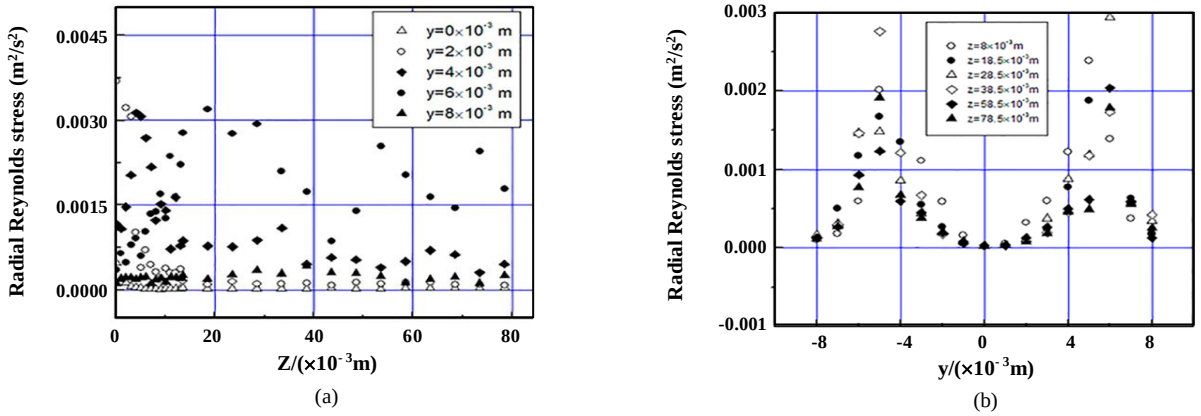

Fig. 5: Radial Reynolds stress varies with heights (a) and horizontal positions.

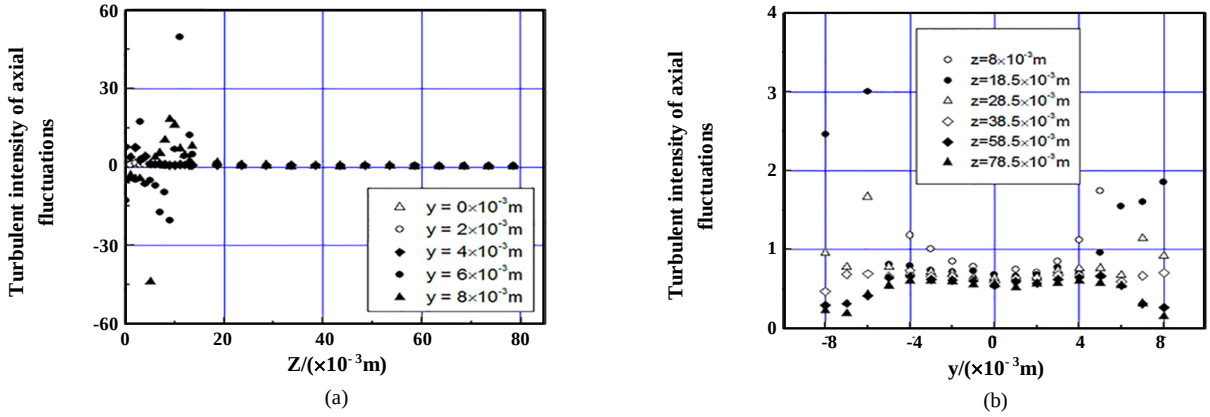

Fig. 6: Axial turbulent intensity varies with height (a) and horizontal distance (b).

turbulent intensity variation with the vertical height and the horizontal distance is given in Fig. 7. It is shown that radial turbulent intensity of the liquid near symmetrical axis mentioned above, waves seriously within the range of bubble formation but changes little in the bubble rising process, compared with the opposite trend for the liquid near the boundary of the bubble channel involved. Furthermore, the radial turbulent intensity is wholly being strengthened with the horizontal distance.

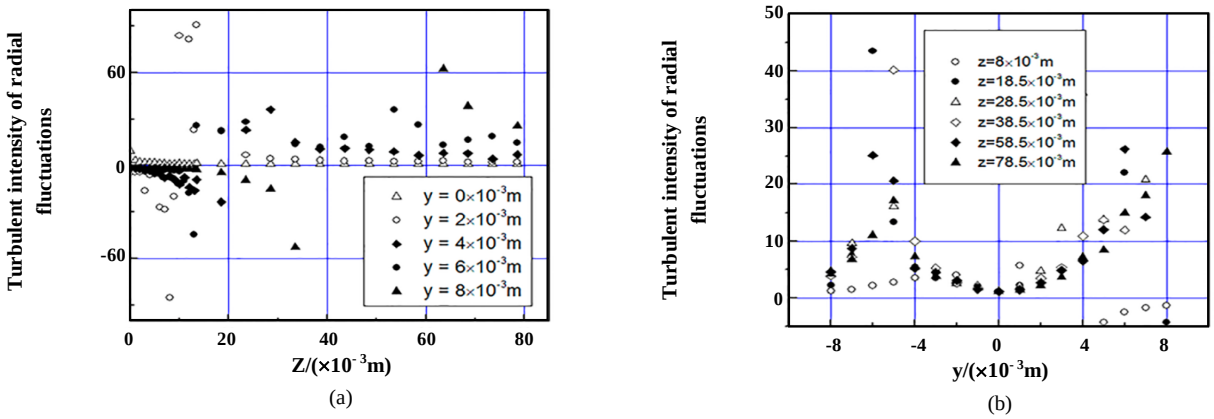

Fig. 7: Radial turbulent intensity varies with height (a) and horizontal distance (b).

CONCLUSIONS

Both liquid instantaneous velocity and mean velocity near single bubble forming and rising in non-Newtonian CMC aqueous solution under low gas flowrate condition have been measured experimentally by **L**aser Doppler **V**elocimetry. The disturbance of fluid surrounding bubble was investigated by means of statistical method, and the conclusions are the following:

During the whole rising process, there might exists a cylindrical channel, vertical to the test section and axisymmetric with the vertical axis line passing through orifice center, since the bubble in the CMC aqueous solution rises steadily along the straight path without any swinging motions. Within the channel, axial Reynolds stress first goes up greatly and then fluctuate toa little extent with the height, but displays symmetrically Gaussian distribution in the horizontal direction. Rradial Reynolds stress almost maintains steady near the channel center, whereas increases slightly and then decreases in the horizontal direction respectively. Especially, within the lower region of bubble formation, turbulent intensity presents lager fluctuation with the height due to the liquid turbulent motion in axial direction compared with that in the region of bubble rise.

Acknowledgement

Authors wish to express their appreciation for the financial support by the National Natural Science Foundation of China (21576214), and Tianjin Natural Science Foundation (16JCYBJC20400).

Nomenclature

H	Test section height, cm
i	The *i*th coincident points
I	Turbulent intensity
n	Flow index
N	Total number of coincident points
O	Origin of the co-ordinate system
u	Velocity component in *x*-axis, m/s
v	Velocity component in *y*-axis, m/s
$\bar{v}$	Mean velocity component in *y*-axis, m/s
v'	Fluctuating velocity in *y*-axis, m/s
$\overline{v'v'}$	Radial Reynolds stress, m^2/s^2
w	Velocity component in *z*-axis, m/s
$\bar{w}$	Mean velocity component in *z*-axis, m/s
w'	Fluctuating velocity in *z*-axis, m/s
$\overline{w'w'}$	Axial Reynolds stress, m^2/s^2
W	Test section width, cm
x	*x*-axis of the co-ordinate system (-)
y	*y*-axis of the co-ordinate system (-)
z	*z*-axis of the co-ordinate system (-)

Greek letters

ρ	Density, kg/m^3
λ	Wave length, nm; time constant, s
η_0	Zero shear viscosity, Pa·s
η_∞	Infinite shear viscosity, Pa·s

Received : Jun. 19, 2017 ; Accepted : Oct. 30, 2017

REFERENCES

[1] Kilonzo P.M., Margaritis, A., The Effects of Non-Newtonian Fermentation Broth Viscosity and Small Bubble Segregation on Oxygen Mass Transfer in Gas-lift Bioreactors: A Critical Review, *Biochem. Eng. J.*, **17**(1): 27-40 (2004).

[2] Rouhi A.R., Fatehifar E., Khazini L., Application of New Inflection Point Method for Hydrodynamics Study in Slurry Bubble Column Reactors, *Iran. J. Chem. Chem. Eng. (IJCCE)*, **32**(2): 81-92 (2013).

[3] Abbaspour A., Khadiv-Parsi P., Khalighi-Sigaroodi F., Ghaffarzadegan R. Optimization of Atropine Extraction Process from Atropa Belladonna by Modified Bubble Column Extractor with Ultrasonic Bath, *Iran. J. Chem. Chem. Eng. (IJCCE)*, **35**(4): 49-60 (2016).

[4] Duineveld P.C., Rise Velocity and Shape of Bubbles in Pure Water at High Reynolds Number, *J. Fluid Mech.*, **292**(1): 325-332 (1995).

[5] Deen N., Van Sint Annaland M., Kuipers J., Multi-scale Modeling of Dispersed Gas-liquid Two-phase Flow, *Chem. Eng. Sci.*, **59**(8-9): 1853-1861 (2004).

[6] Kulkarni A.A., Joshi J.B., Bubble Formation and Bubble Rise Velocity in Gas-liquid Systems: A Review, *Ind. Eng. Chem. Res.*, **44**(16): 5873-5931 (2005).

[7] Räbiger N., Vogelpohl A., "Encyclopedia of Fluid Mechanics", Gulf Pub. Co., Houston (1986).

[8] Acharya A., Mashelkar R.A., Ulbrecht J.J., Bubble Formation in Non-Newtonian Liquids, *Ind. Eng. Chem. Fundamen.*, **17**(3): 230-232 (1978).

[9] Acharya A., Ulbrecht J.J., Note on the Influence of Viscoelasticity on the Coalescence Rate of Bubbles and Drops, *AIChE J.*, **24**(2): 348-351 (1978).

[10] Terasaka K., Tsuge H., Bubble Formation at a Single Orifice in Non-Newtonian Liquids, *Chem. Eng. Sci.*, **46**(1): 85-93 (1991).

[11] Terasaka K., Tsuge H., Bubble Formation at Orifice in Viscoelastic Liquids, *AIChE J.*, **43**(11): 2903-2910 (1997).

[12] Terasaka K., Tsuge H., Bubble Formation at a Nozzle Submerged in Viscous Liquids Having Yield Stress, *Chem. Eng. Sci.*, **56**(10): 3237-3245 (2001).

[13] Li H.Z., Bubbles in Non-Newtonian Fluid: Formation, Interactions and Coalescence, *Chem. Eng. Sci.*, **54**(13-14): 2247-2254 (1999).

[14] Li H.Z., Mouline Y., Midoux N., Modeling the Bubble Formation Dynamics in Non-Newtonian Fluids, *Chem. Eng. Sci.*, **57**(3): 339-346 (2002).

[15] Favelukis M., Albalak R.J., Bubble Growth in Viscous Newtonian and Non-Newtonian Liquids, *Chem. Eng. J. Biochem. Eng. J.*, **63**(3): 149-155 (1996).

[16] Burman J.E., Jameson G.J., Growth of Spherical Gas Bubbles by Solute Diffusion in Non-Newtonian (Power law) Liquids, *Int. J. Heat Mass Transfer*, **21**(2): 127-136 (1978).

[17] Martín M., Montes F.J., Galán M.A., Numerical Calculation of Shapes and Detachment Times of Bubbles Generated from a Sieve Plate, *Chem. Eng. Sci.*, **61**(2): 363-369 (2006).

[18] Martín M., Montes F.J., Galán M.A., On the Influence of the Liquid Physical Properties on Bubble Volumes and Generation Times, *Chem. Eng. Sci.*, **61**(16): 5196-5203 (2006).

[19] Ma Y.G. Fan W.Y., Jiang S.K., Zhu C.Y., Li H.Z., Modified Model of Bubble Formation in Non-Newtonian Fluids, *Trans. Tianjin Univ.*, **15**(1): 56-60 (2009).

[20] Vélez-Cordero J.R., Zenit R., Bubble Cluster Formation in Shear-thinning Inelastic Bubbly Columns, *J. Non-Newtonian Fluid Mech.*, **166**(1-2): 32-41 (2011).

[21] Hassager O., Negative Wake behind Bubbles in Non-Newtonian Liquids, *Nature*, **279**: 402-403 (1979).

[22] Bisgaard C., Hassager O., An Experimental Investigation of Velocity Fields around Spheres and Bubbles Moving in Non-Newtonian Liquid, *Rheol. Acta*, **21**(4-5): 537-548 (1982).

[23] Arigo M.T., McKinley G.H., An Experimental Investigation of Negative Wakes behind Spheres Settling in a Shear-thinning Viscoelastic Fluid, *Rheol. Acta*, **37**(4): 307-327 (1998).

[24] Frank X., Li H.Z., Complex Flow around a Bubble Rising in a Non-Newtonian Fluid, *Phys. Rev. E*, **71**(3): 036309 (2005).

[25] Frank X., Li H.Z., Negative Wake behind a Sphere Rising in Viscoelastic Fluids: A Lattice Boltzmann Investigation, *Phys. Rev. E*, **74**(5): 056307 (2006).

[26] Sousa R.G., Pinto A.M.F.R., Campos J.B.L.M., Interaction Between Taylor Bubbles Rising in Stagnant Non-Newtonian Fluids, *Int. J. Multiphase Flow*, **33**(9): 970-986 (2007).

[27] Lin T.J., Lin G.M., Mechanisms of In-line Coalescence of Two-unequal Bubbles in a Non-Newtonian Fluid, *Chem. Eng. J.*, **155**(3): 750-756 (2009).

[28] Fan W.Y., Ma Y.G., Li X.L., Li H.Z., Study on the Flow Field around Two Parallel Moving Bubbles and Interaction Between Bubbles Rising in CMC Solutions by PIV, *Chin. J. Chem. Eng.*, **17**(6): 904-913 (2009).

[29] Kumara W.A.S., Elseth G., Halvorsen B.M., Melaaen M.C., Comparison of Particle Image Velocimetry and Laser Doppler Anemometry Measurement Methods Applied to the Oil-water Flow in Horizontal Pipe, *Flow Meas. Instrum.*, **21**(2): 105-117 (2010).

[30] Fan W.Y., Yin X.H., A Laser Imaging-LDV Coupling Measurement of Single Bubble Forming and Rising in Shear-thinning Fluid, *J. Therm. Sci.*, **23**(3): 233-238 (2014).